

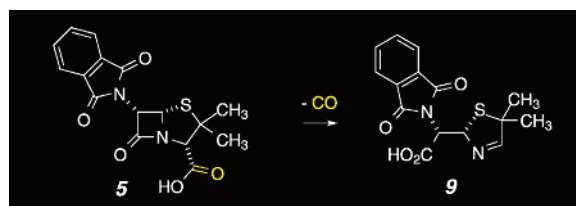
## A Thermal Decarbonylation of Penam $\beta$ -Lactams

Keith W. Wiitala, Zhixin Tian, Christopher J. Cramer, and Thomas R. Hoye\*

Department of Chemistry and Supercomputer Institute, University of Minnesota,  
207 Pleasant Street SE, Minneapolis, Minnesota 55455-0431

hoye@chem.umn.edu

Received November 3, 2007



Penam acids **6–8** [i.e., (2*S*,5*R*,6*R*)-, (2*S*,5*S*,6*R*)-, and (2*S*,5*R*,6*S*)-isomers of 6-(1,3-dihydro-1,3-dioxo-2*H*-isoindol-2-yl)-3,3-dimethyl-7-oxo-4-thia-1-azabicyclo[3.2.0]heptane-2-carboxylic acid] were prepared by deesterification of the corresponding methyl esters **2–4**. The same methodology applied to ester **1** did not lead to the (2*S*,5*S*,6*S*)-isomer **5** but rather a 72% yield of the thiazoline derivative **9**. High-resolution mass spectrometry analysis of the reaction headspace gases indicated that a stoichiometric amount of carbon monoxide is produced during the deesterification of **1**. A mechanism for this decarbonylation reaction is proposed. This appears to represent a new type of fragmentation reaction for a penam carboxylic acid. The free energies of various reaction species along viable decarbonylation reaction coordinates for acids **5** and **7** were computed by using the density functional theory method IEFPCM/M06/6-31+G(d). Anionic and zwitterionic (neutral) variants of the proposed mechanism were considered, but each produced computed activation free energies deemed to be too high (>45 kcal/mol) to be experimentally relevant. The computed activation free energies for the protonated (cationic) variant of the mechanism were 17.3 kcal/mol for **7** vs 8.8 kcal/mol for **5**. The value of this difference in energies of activation ( $\Delta\Delta G^\ddagger$ ) is quite consistent with experimental observations and supports the proposed mechanism. For a portion of the computed reaction coordinate that involves ring opening of the lactam ring by an internal carboxylic acid group to form a cyclic anhydride, the expected tetrahedral intermediate was circumvented by a direct (concerted) and facile *N*- to *O*-acyl migration event. Additional thermal gas-phase reaction products produced during gas chromatographic analysis of the penams **1–8** were characterized with high-resolution mass spectrometry, and possible mechanisms for their formation are presented.

### Introduction

Recently, we evaluated the abilities of some density functional theory (DFT) methods to discriminate between diastereomers using experimental and computed NMR chemical shifts and penam  $\beta$ -lactams **1–8** (Figure 1) as a test set.<sup>1</sup> These compounds were prepared by using established methods.<sup>2–4</sup> In particular, the methyl esters **1–4** were cleaved to the corresponding acids

**5–8** by using LiI in refluxing ethyl acetate. This allowed for the isolation of **6–8**. However, the carboxylic acid **5** from the corresponding methyl ester **1** was not isolable; instead, the thiazoline **9** was obtained as the major product. Ugi<sup>5</sup> and Baldwin,<sup>6</sup> using different methods and precursors, have previously synthesized *ent*-**9**. This unusual (and new) decarbonylation was also observed from the (2*S*,5*S*,6*R*)-acid **7** (~20% conversion after 2 days of heating to reflux in EtOAc) but not from **6** and **8** under the same conditions.

(1) Wiitala, K. W.; Cramer, C. J.; Hoye, T. R. *Magn. Reson. Chem.* **2007**, *45*, 819–829.

(2) Kukulja, S. *J. Am. Chem. Soc.* **1971**, *93*, 6267–6269.

(3) Fekner, T.; Baldwin, J. E.; Adlington, R. M.; Jones, T. W.; Prout, C. K.; Schofield, C. J. *Tetrahedron* **2000**, *56*, 6053–6074.

(4) Fisher, J. W.; Trinkle, K. L. *Tetrahedron Lett.* **1994**, *35*, 2505–2508.

(5) (a) Schutz, A.; Ugi, I. *J. Chem. Res. (S)* **1979**, 157. (b) Schutz, A.; Ugi, I. *J. Chem. Res. (M)* **1979**, 2064–2071.

(6) Baldwin, J. E.; Chan, R. Y.; Sutherland, J. D. *Tetrahedron Lett.* **1994**, *35*, 5519–5522.

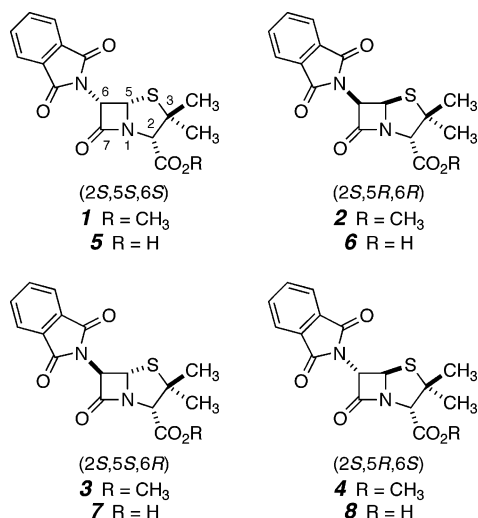
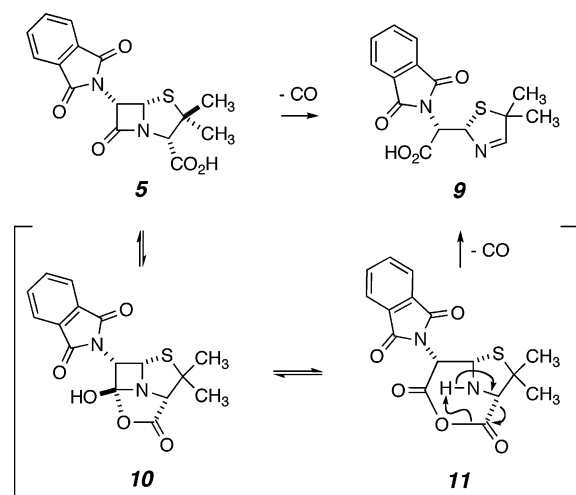


**FIGURE 1.** Structures of the diastereomeric penam  $\beta$ -lactam esters (**1–4**) and acids (**5–8**) studied.

### SCHEME 1



Thiazoline **9** formally results from the loss of carbon monoxide from the acid **5** (Scheme 1, top). Because the chemical reactivities of  $\beta$ -lactam antibiotics (e.g., penams and cepham) have been studied so extensively,<sup>7</sup> we were surprised to discover that this transformation represents an apparently new mode of reactivity for a penam carboxylic acid. Herein, we report our findings.

This paper is organized as follows. The isolation and quantification of carbon monoxide is presented, along with a mechanistic hypothesis. Then the results of computational studies used to probe the viability of such a mechanism are discussed. Finally, we propose structures and mechanisms for some additional thermal gas-phase reaction products that are produced during gas chromatographic analysis of the penams **1–8**.

## Results and Discussion

**Decarbonylation Experiments.** The production of carbon monoxide (CO) in the conversion of **5** (or its lithium carboxylate) to **9** was verified by mass spectrometric analysis of the

(7) E.g., twenty-seven thousand reactions appear from a Beilstein search of fused bicyclic  $\beta$ -lactam reactants.

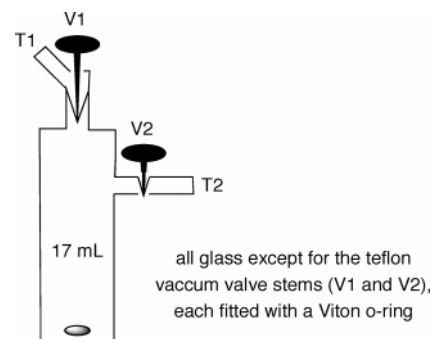


**FIGURE 2.** Apparatus used to perform HRMS headspace analysis of the penam decarbonylation reaction.

headspace of the deesterification reaction of **1** (LiI, EtOAc, 80 °C). To account for this outcome, we proposed, as the working hypothesis, a mechanism that had the essential elements shown further in Scheme 1. The anhydride **11**, derived from intramolecular opening of the  $\beta$ -lactam in **5** by the carboxylic acid group via the tetrahedral intermediate **10**,<sup>8</sup> could thermally eject CO. It is interesting that this mechanism is directly parallel to that of an analogous reverse reaction—namely the Ugi penicillin synthesis.<sup>5,9</sup> In that process the acid **9**, for example, reacts with an isonitrile (isoelectronic with CO) to produce an amide corresponding to acid **5**.

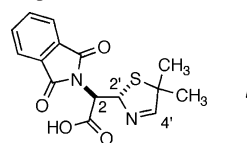
To quantify the amount of CO produced, isotopically labeled <sup>13</sup>CO (4.5 mL) was introduced as an internal standard into the reaction apparatus immediately before it was heated. Subsequent mass spectral analysis indicated the production of ca. 99% of the theoretical amount of CO. Conventional workup of this reaction mixture led to a 72% isolated yield of **9** and indicated that no starting ester **1** remained.

For the less reactive (and isolable) acid **7** a qualitative headspace analysis (HRMS, Figure 2) also showed the presence of carbon monoxide. When **7** was heated on a hot stage (mp 95–98 °C), vigorous bubbling was observed above 100 °C and had finished when the sample had reached 155 °C several minutes later. When this melting point slide was cooled, the material resolidified. Remeasurement of the melting behavior of this new solid showed a mp of 110–114 °C, and there was no additional gas evolution observed.<sup>10</sup> These observations are consistent with a thermal decarbonylation reaction, the onset of which is enabled once acid **7** leaves its lattice and enters the melt. By contrast, acids **6** and **8** did not show any unusual thermal reactivity behavior in the melt or in solution. This is consistent with the mechanistic ideas shown in Scheme 1; the

(8) For examples of other reactions initiated by intramolecular attack on the lactam carbonyl by a B-ring hydroxyl group (alcohol) see: (a) Gutowski, G. E.; Daniels, C. M.; Cooper, R. D. G. *Tetrahedron Lett.* **1971**, 3429–3432. (b) Baldwin, J. E.; Cobb, J. E.; Sheppard, L. N. *Tetrahedron* **1987**, 43, 1003–1012.

(9) Ugi, I. *Angew. Chem., Int. Ed. Engl.* **1982**, 21, 810–819.

(10) The <sup>1</sup>H NMR (CDCl<sub>3</sub>, 500 MHz)  $\delta$  1.59 (s, 3H, Me), 1.64 (s, 3H, Me), 4.82 (d, 1H, *J* = 10.8 Hz, H<sub>2</sub>), 6.65 (dd, 1H, *J* = 10.8, 2.2 Hz, H<sub>2'</sub>), 7.42 (d, 1H, *J* = 2.2 Hz, H<sub>4'</sub>), 7.8 (m, 2H, A<sub>meta</sub>), 7.9 (m, 2H, A<sub>ortho</sub>) and LCMS [*t*<sub>R</sub> = 14.5 min ( $\neq t_{R9}$  = 12.4 min); ESI/APCI mixed mode (neg ion) *m/e* 317 amu] data obtained for this material are consistent with its formulation as **i**, the C2-epimer of **9**



significantly puckered nature of the  $\beta$ -lactam ring in the fused bicyclic penam skeleton places the carboxylic acid essentially in the plane of the lactam carbonyl group, which makes the formation of intermediates analogous to **10** and **11** improbable because of the poor attack trajectory.

**Computational Studies.** To explore whether the proposed decarbonylation reaction pathway (Scheme 1) is energetically reasonable, we computed various likely intermediates and some of the associated transition states for their interconversion. Since decarbonylation was observed under several different experimental conditions (LiI, EtOAc at reflux for **5**; EtOAc at reflux for **7**; and neat melt for **7**) it is not possible to know the exact state of protonation of the key event(s). Therefore, anionic, neutral, and cationic pathways were explored for both **5** and **7**. That is, we considered pathways beginning from the carboxylate, from the neutral carboxylic acid capable of tautomerizing to zwitterionic intermediates, and from the protonated substrate, recognizing what can occur at various sites. We did not enforce a unimolecular pathway for interconversion between any tautomeric pairs. The phthalimido moieties in **5** and **7** were replaced by maleimido substructures to enhance computational efficiency. We will refer to these truncated structures as **5'** and **7'**, respectively.

For the characterization of the various decarbonylation reaction coordinates, the geometry of each molecular structure was fully optimized in the gas phase at the density functional level of theory using the M06 hybrid meta-generalized gradient approximation functional<sup>11</sup> and the 6-31+G(d) basis set.<sup>12</sup> Aqueous free energies for each minimum and maximum were then recomputed by using the IEFPCM solvation model<sup>13</sup> with default united-atom radii. To assess the maximum effects of polar solvation, the continuum model for water was chosen as a matter of convenience. The choice of solvent modeled has only a small effect on relative energies. For example, the computed free energy difference between **5'f** and **5'e** was 4.0 kcal/mol in water and 4.6 kcal/mol in THF while the computed free energy difference between **7'f** and **7'e** was 17.3 kcal/mol in water and 15.4 kcal/mol in THF. Analytical vibrational frequencies were computed in order to assign the nature of all stationary points as either minima or transition state (TS) structures and also to compute thermal contributions to 298 K isomer enthalpies.<sup>14</sup>

Solvation free energies were summed with gas-phase enthalpies to generate composite free energies in aqueous solution (gas-phase thermal contributions to free energies had no significant influence on relative isomer energetics, but were judged to be of limited utility based on the sensitivity of computed entropies to low-frequency vibrations in the quantum-mechanical harmonic-oscillator approximation<sup>14</sup>). A pruned (75 302) integration grid containing 75 radial shells and 302 angular points per shell (approximately 7 000 points for each atom) was used on each atom. Density functional calculations were carried out by using the Gaussian 03 suite of electronic structure programs.<sup>15</sup>

(11) Zhao, Y.; Truhlar, D. G. *Theor. Chem. Acc.* Online First [doi:10.1007/s00214-007-0310-x].

(12) Hehre, W. J.; Radom, L.; Schleyer, P. v. R.; Pople, J. A. *Ab Initio Molecular Orbital Theory*; Wiley: New York, 1986; p 82.

(13) Miertus, S.; Scrocco, E.; Tomasi, J. *Chem. Phys.* **1981**, *55*, 117–129.

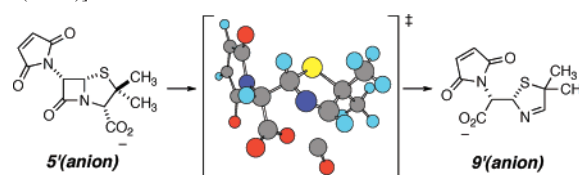
(14) Cramer, C. J. *Essentials of Computational Chemistry: Theories and Models*, 2nd ed.; John Wiley & Sons: Chichester, UK, 2004; pp 334–366.

The reaction pathways for anionic<sup>16a</sup> and neutral<sup>16b</sup> forms of **5'** and **7'** were explored and found to have transition states too high in energy to be relevant. By contrast, protonated structures provided reaction coordinates (Figures 3 and 4) consistent with the experimental observation of decarbonylation. In each case, we considered protonation of the lactam at two sites and found that the tautomer derived from *N*-protonation (**5'b** or **7'b**) was lower in free energy than that derived from *O*-protonation (**5'a** or **7'a**, see Table 1), owing in part, presumably, to the pyramidalization of the nitrogen atom enforced by the penam ring system. In the case of **7'**, the *N*-protonated tautomer **7'b** is additionally stabilized by hydrogen bonding to a carbonyl oxygen of the maleimide moiety. From the *N*-protonated tautomer, TS structures **5'c** or **7'c** for ring opening to the corresponding protonated anhydrides **5'd** or **7'd** were found. The activation free energies of each of these steps were small (8.3 and 9.1 kcal/mol, respectively). Surprisingly and interestingly, the computational results for the cationic pathway indicated a low-energy transition state for the direct conversion (i.e., without an intermediate) of both **5'b** to **5'd** and **7'b** to **7'd**. This process is in distinct contrast to that involving a classical tetrahedral intermediate (i.e., the *N*-protonated analogue of **10**) analogous to our initial mechanistic hypothesis (cf. Scheme 1). Finally, no energetically viable paths involving the *O*-protonated species **5'a** or **7'a** were found.<sup>17</sup>

The anhydrides themselves are also subject to a tautomeric equilibrium associated with which carbonyl oxygen is protonated; in order to lose carbon monoxide, there must be a proton

(15) Frisch, M. J.; Trucks, G. W.; Schlegel, H. B.; Scuseria, G. E.; Robb, M. A.; Cheeseman, J. R.; Montgomery, J. A.; Vreven, T.; Kudin, K. N.; Burant, J. C.; Millam, J. M.; Iyengar, S. S.; Tomasi, J.; Barone, V.; Mennucci, B.; Cossi, M.; Scalmani, G.; Rega, N.; Petersson, G. A.; Nakatsuji, H.; Hada, M.; Ehara, M.; Toyota, K.; Fukuda, R.; Hasegawa, J.; Ishida, M.; Nakajima, T.; Honda, Y.; Kitao, O.; Nakai, H.; Klene, M.; Li, X.; Knox, J. E.; Hratchian, H. P.; Cross, J. B.; Adamo, C.; Jaramillo, J.; Gomperts, R.; Stratmann, R. E.; Yazyev, O.; Austin, A. J.; Cammi, R.; Pomelli, C.; Ochterski, J. W.; Ayala, P. Y.; Morokuma, K.; Voth, G. A.; Salvador, P.; Dannenberg, J. J.; Zakrzewski, V. G.; Dapprich, S.; Daniels, A. D.; Strain, M. C.; Farkas, O.; Malick, D. K.; Rabuck, A. D.; Raghavachari, K.; Foresman, J. B.; Ortiz, J. V.; Cui, Q.; Baboul, A. G.; Clifford, S.; Cioslowski, J.; Stefanov, B. B.; Liu, G.; Liashenko, A.; Piskorz, P.; Komaromi, I.; Martin, R. L.; Fox, D. J.; Keith, T.; Al-Laham, M. A.; Peng, C. Y.; Nanayakkara, A.; Challacombe, M.; Gill, P. M. W.; Johnson, B.; Chen, W.; Wong, M. W.; Gonzalez, C.; Pople, J. A. *Gaussian 03, Revision D.01*; Gaussian, Inc.: Pittsburgh, PA, 2004.

(16) (a) For the anionic reaction pathways for **5'** and **7'**, reactant structures and TS structures corresponding to loss of carbon monoxide could be located, but no intermediate structures could be found. Attempts to generate, for example, intermediates associated with ring opening of the lactam following attack of the carboxylate on the amide carbonyl led smoothly back to reactants. Thus, lactam ring opening is computed to occur with concerted loss of carbon monoxide [e.g., see TS in brackets for **5'**(anion) to **9'**(anion)]



However, the computed activation free energies for the reactions of each of **5'** and **7'** are in excess of 45 kcal/mol, suggesting that the anionic reaction does not play a significant role in the observed decarbonylations. (b) In the cases of neutral **5'** and **7'**, bicyclic anhydrides formed by ring opening of the lactam together with proton transfer from the carboxylic acid to the 1,3-thiazolidine were identified as stable intermediates having free energies of 4.2 and 18.4 kcal/mol relative to precursors **5'** and **7'**, respectively. Decarbonylation TS structures that produce zwitterionic thiazolinium carboxylate products could be located. Again, however, the computed free energies of activation were too high to be experimentally relevant: 53.7 and 59.4 kcal/mol for **5'** and **7'**, respectively.

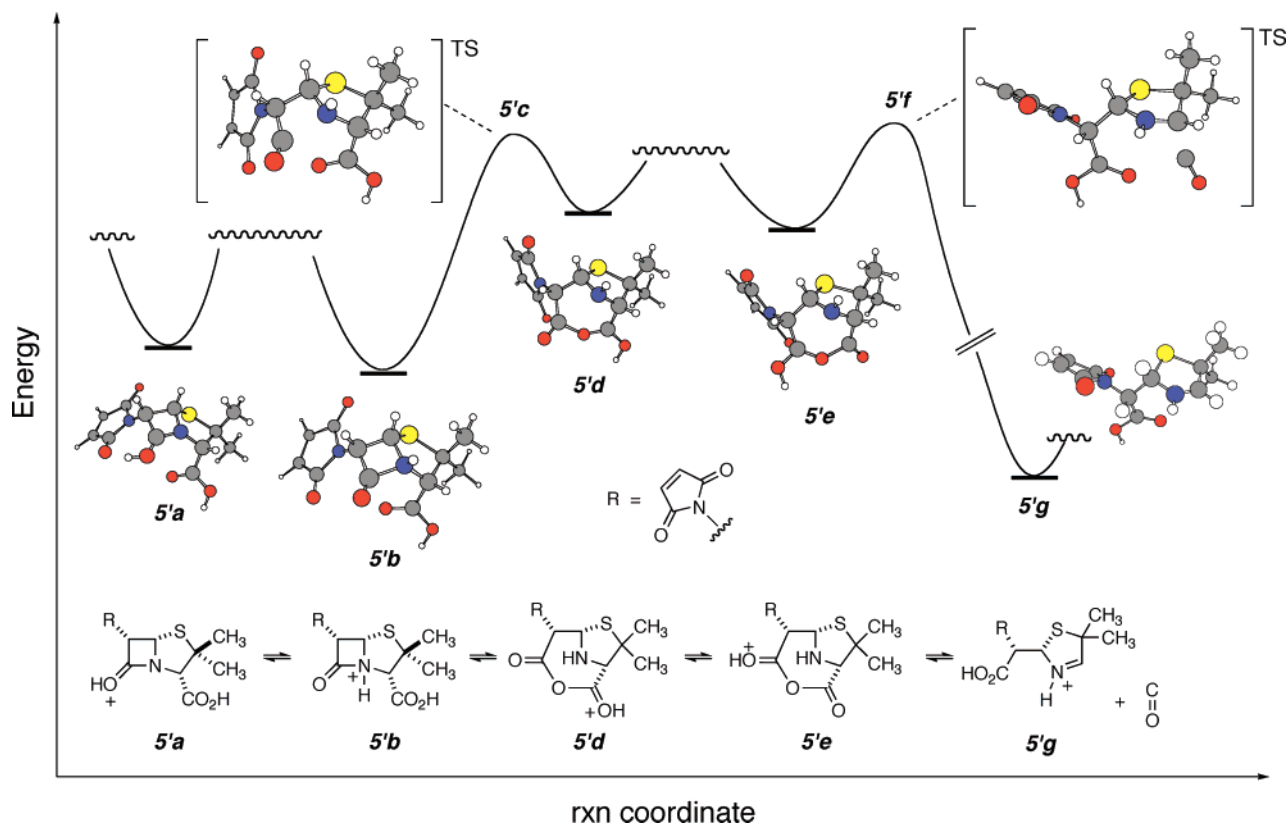


**FIGURE 3.** Reaction coordinate for decarboxylation of **5'** computed at the IEFPCM/M06/6-31+G(d) level. Positions of local minima and TS structures with ball-and-stick stereodepictions for **5'a–f** are to scale in energy along the vertical coordinate (see Table 1 for values).

transfer from the carbonyl deriving from the original carboxylic acid to the carbonyl deriving from the original  $\beta$ -lactam. In the case of **5'**, these two tautomers (i.e., **5'd** and **5'e**) are within 0.7 kcal/mol of one another. In the case of **7'**, on the other hand, the second anhydride tautomer is not a minimum; rather it settles to the tetrahedral intermediate **7'e** that is 11 kcal/mol more stable than the first protonated anhydride (**7'd**). The hydrogen bonding of the thiazolidine secondary amine to the maleimide renders the nitrogen lone pair sufficiently nucleophilic that it adds to the protonated carbonyl of the putative second anhydride tautomer to generate a particularly stable tricyclic intermediate **7'e**.

Decarboxylation TS structures **5'f** or **7'f**, converting intermediates **5'e** or **7'e** to **5'g** or **7'g**, were located in each case. For **5'**, the activation free energy relative to the initial *N*-protonated lactam **5'b** (the global minimum on the reaction coordinate) is computed to be only 8.8 kcal/mol. Thus, the overall decarboxylation would be expected to proceed very rapidly (consistent with the fact that acid **5** was not isolable), provided that proton-transfer reactions to interconvert the various tautomers are facile (we did not attempt to locate such structures, since we expect bimolecular proton transfers likely to be more relevant than unimolecular ones).

(17) The zwitterionic (i.e., neutral) tetrahedral intermediate **10** formed from attack of the carboxylate anion on the O-protonated lactam carbonyl could be located as a minimum. However, when a proton was then added to the lactone carbonyl oxygen atom in **10**, i.e., generating the same tetrahedral intermediate that would be created from attack of the neutral carboxylic acid on the O-protonated lactam, the resulting polycyclic structure reverts without barrier to **5'a** again. Thus, the combination of strain and good leaving-group character of the  $-\text{CO}_2\text{H}$  moiety prevents a pathway via **5'a** from being a viable mechanistic alternative.

For **7'**, decarboxylation has a larger activation free energy, 17.3 kcal/mol, because of the significant stability of the tricyclic intermediate **7'e** (note that the value of 13.9 kcal/mol in Table 1 for this TS structure is relative to the *N*-protonated lactam **7'b**, but the tricyclic intermediate **7'e** is more stable than the lactam, accounting for the higher activation free energy). This greater barrier to reaction is consistent with the experimental observation that decarboxylation of diastereomer **7** is slower than that of **5**. We note that the orthoaminal that would derive from deprotonation of the tricyclic intermediate **7'e** would be expected to be unstable; its ring opening to reform **7**, based on our computations on the neutral system, should be facile so it is unsurprising that tricyclic compounds are not isolated experimentally.

Finally, it should be restated that these activation barriers (8.8 vs 17.3 kcal/mol) are for the *protonated forms* of **5'** and **7'**, respectively. The most important feature is the *relative* values of the two computed barriers. The observed rate of each reaction is, of course, the product of its rate constant *and* the concentration of the protonated species; the latter is not known, but would likely be very small. Thus, the observed time courses for the decarboxylation reactions of **5** and **7** are entirely consistent with the (otherwise small) computed activation barriers.

**Other Thermal Reactions (via GC-MS Analysis).** In addition to the decarboxylation product **9** discussed above, evidence for additional products from thermal decomposition of the penams was obtained during gas chromatographic analysis, more specifically by GC-MS. For example, each of the methyl ester penams **1** through **4** underwent a retro [2+2] reaction to produce the thiazolidine methyl ester **12** ( $M^+ = 173.0$  amu,  $t_R = 6.93$  min).<sup>18</sup> Under some conditions, **12** was the only

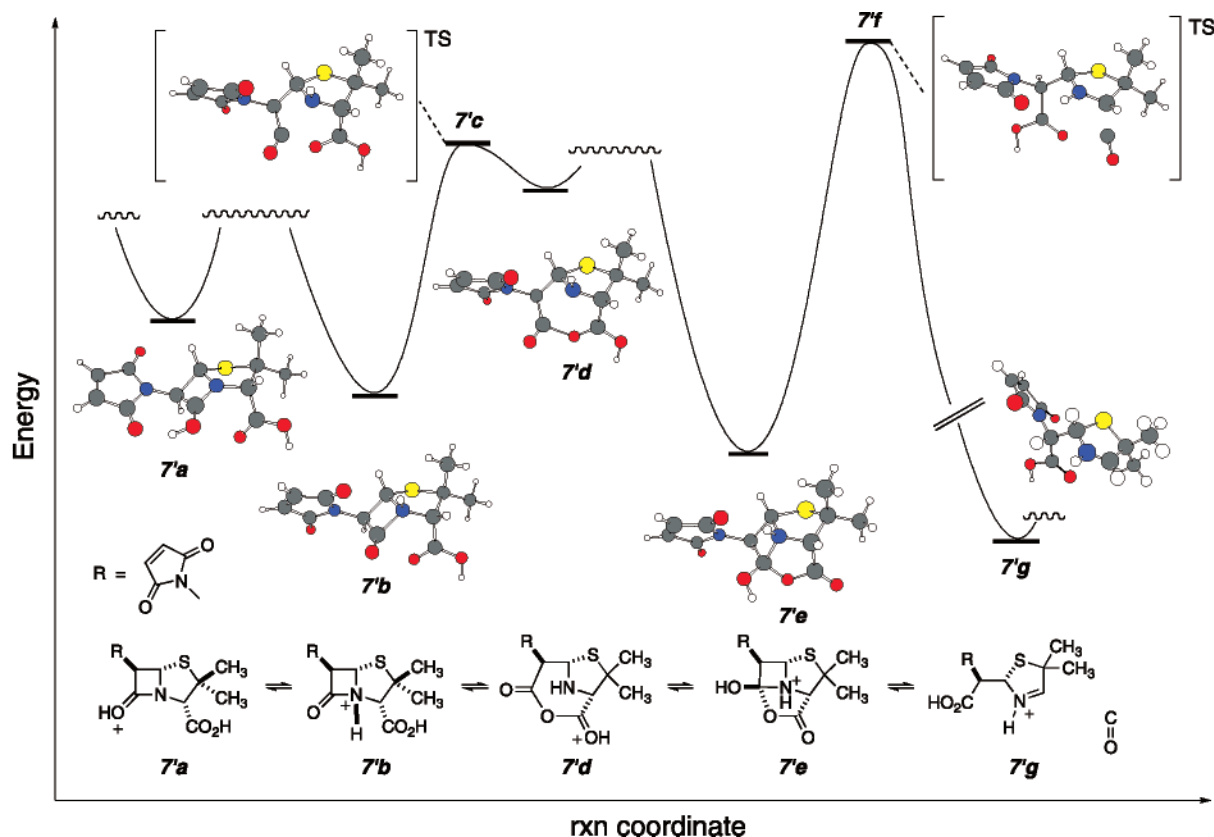
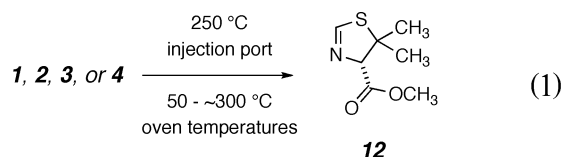


**FIGURE 4.** Reaction coordinate for decarbonylation of **7'** computed at the IEFPCM/M06/6-31+G(d) level. Positions of local minima and TS structures with ball-and-stick stereodepictions for **7'a–f** are to scale in energy along the vertical coordinate (see Table 1 for values).

**TABLE 1.** IEFPCM/M06/6-31+G(d) Free Energies (kcal/mol) Relative to *N*-Protonated Lactams (**b**) for Stationary Points along Protonated Decarbonylation Reaction Coordinates of **5'** and **7'**

| acid isomer | stationary point                        |   |                             |                         |                                      |                                |   |
|-------------|---|---|-----------------------------|-------------------------|--------------------------------------|--------------------------------|---|
|             | <b>a</b><br><i>O</i> -protonated lactam | <b>b</b><br><i>N</i> -protonated lactam | <b>c</b><br>ring-opening TS | <b>d</b><br>anhydride I | <b>e</b><br>anhydride II or Tricycle | <b>f</b><br>decarbonylation TS | <b>g</b><br><i>N</i> -protonated thiazoline |
| <b>5'</b>   | 0.9                                     | 0.0                                     | 8.3                         | 5.7                     | 4.8                                  | 8.8                            | −18.5                                       |
| <b>7'</b>   | 2.9                                     | 0.0                                     | 9.1                         | 7.6                     | −3.4                                 | 13.9                           | −14.0                                       |

compound eluted, while under others, both **12** and the starting ester were observed. Thiazoline **12** (eq 1) and all of the compounds presented next in Table 2 (**13–19**) were only produced under the conditions of the GC analysis; none were isolated; their structures/identity are inferred principally from their mass spectral features (both electron impact and chemical ionization).



The acids **6–9** have richer manifolds of thermal reaction pathways compared to the methyl esters. The structures assigned to or identified as the products of these decomposition events are shown as **13–19** in Table 2. These are presented in order

of increasing retention time (i.e., ca. increasing boiling point on the DB-5MS columns used for GC analysis). In each of the following several paragraphs we suggest possible mechanistic pathways by which these products might arise. We assume all to be unimolecular, gas-phase processes.

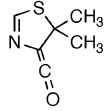
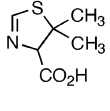
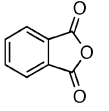
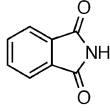
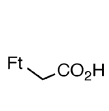
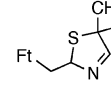
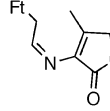
Thiazolines **13** and **14** and phthalimidoacetic acid (**17**) could all come from a common intermediate, namely the acyliminium ion **20** arising from initial C5–C6 fragmentation in the starting penam acid (Scheme 2). This could either fragment directly to **14** (cf. formation of **12** from esters **1–4**) or, following proton transfer to produce **21**, internal acylation of the carboxylate in **21** would give the mixed anhydride **22**. Thermal elimination would then produce **13** and **17**.

Isolated, decarbonylated acid **9** was also observed to undergo thermal degradation, and the products are indicated in Table 2 (final row). Simple decarboxylation of **9**, a preceded process,<sup>19</sup> gives the thiazoline **18** (Scheme 3). Phthalimide (**16**, Ft-H) can arise from 1,2- (or *vicinal*) elimination in **9** (or the related

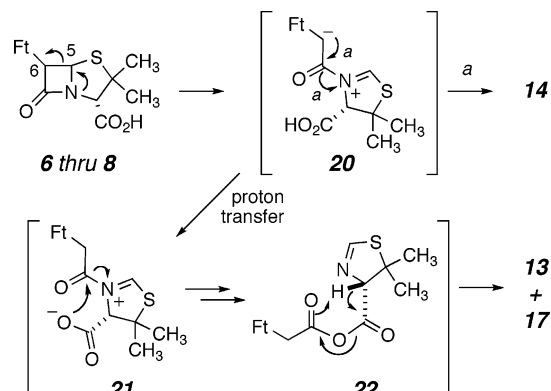
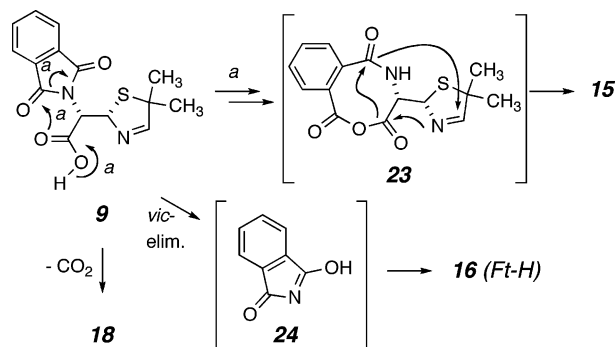
(18) (a) Bell, M. R.; Carlson, J. A.; Oesterlin, R. *J. Org. Chem.* **1972**, *37*, 2733–2735. (b) Sharma, R.; Stoodley, R. *J. Chem. Soc., Perkin Trans. I* **1980**, 2001–2008.

(19) (a) Sheehan, J. C.; Cruickshank, P. A. *J. Am. Chem. Soc.* **1956**, *78*, 3677–3680. (b) Sheehan, J. C.; Schneider, J. A. *J. Org. Chem.* **1966**, *31*, 1635–1637.

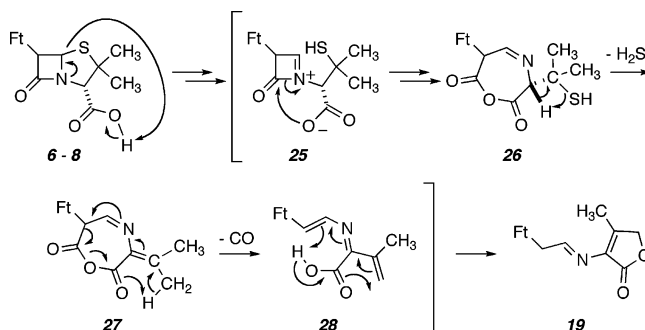
**TABLE 2.** Structures and Relative Amounts of Thermal Decomposition Products Observed upon Subjection of Penam Acids 6–8 (and Thiazoline Acid 9) to GC-MS Analysis<sup>a,b</sup>

| Analyte (Acid) | Thermal Products  |   |   |  |  |  |  |
|----------------|---|---|---|--|--|--|--|
|                |          |  |                    |                     |  |                                     |                                     |
|                | <b>13</b><br>RT = 7:18 min<br>141.0234<br>(10.5 ppm)<br>C <sub>8</sub> H <sub>7</sub> SNO | <b>14</b><br>RT = 7:46 min<br>159.2   | <b>15</b><br>RT = 8:14 min<br>148.0153<br>(5.2 ppm)<br>C <sub>8</sub> H <sub>4</sub> O <sub>3</sub> | <b>16</b><br>RT = 9:23 min<br>147.0310<br>(6.9 ppm)<br>C <sub>8</sub> H <sub>5</sub> NO <sub>2</sub> | <b>17</b><br>RT = 11:58 min<br>205.1   | <b>18</b><br>RT = 13:53 min<br>274.0755<br>(7.7 ppm)<br>C <sub>14</sub> H <sub>14</sub> SN <sub>2</sub> O <sub>2</sub> | <b>19</b><br>RT = 14:26 min<br>284.0812<br>(-5.1 ppm)<br>C <sub>13</sub> H <sub>12</sub> N <sub>2</sub> O <sub>4</sub> |
| <b>6</b>       | 7   | 18  | 6   | 4  | 0  | 53   | 6  |
| <b>7</b>       | 13  | 48  | 1   | 2  | 7  | 20   | 9  |
| <b>8</b>       | 21  | 47  | 5   | 6  | 2  | trace  | 19   |
| <b>9</b>       | 0   | 0   | 7   | 7  | 0  | 76   | 0  |

<sup>a</sup> Relative amounts expressed as percentages of total peak area in EI GC(MS) chromatogram. <sup>b</sup> Ft = phthalimido.

**SCHEME 2****SCHEME 3**

iminium carboxylate zwitterions) to produce the transient tautomer **24** en route to **16**. Phthalic anhydride (**15**) could arise via the ring-expanded, cyclic anhydride **23**, the product of internal ring opening of the imide by the free carboxylic acid in **9**. The fact that **18** was also produced during GC analysis of the penam acids **6** or **7** suggests that the facile decarbonylation

**SCHEME 4**

of **5** occurs, albeit more slowly, for these diastereomers as well to produce either *ent*-**9** (from **6**) or *epi*-**9** (from **7**) as intermediates, which proceed on to **18** by decarboxylation.

The final degradation product, for which we suggest the structure of lactone **19** (Table 2), is common to each of the penam acids **6–8** but not to thiazoline **9**. Its composition (loss of CO and H<sub>2</sub>S) is clear from CI-HRMS data, but its exact constitution is tentative, since its EI-MS fragmentation is dominated by formation of FtCH<sub>2</sub><sup>+</sup> (base peak); the only other significant ion observed was assigned the structure FtCH<sub>2</sub>-CH=NH<sup>+</sup>. That the same compound (identical MS and GC retention time data) is formed from each of the diastereomers **6–8** is consistent with the fact that compound **19** is nondiastereomeric.

The essential features of a possible mechanism for a decarbonylation/dehydrosulfuration pathway are shown in Scheme 4. Initial opening of the thiazolidine ring forms the diastereomeric acyliminium zwitterions **25**, which can ring-expand to the anhydrides **26**. The subsequent unimolecular thermal 1,2-elimination of hydrogen sulfide to form **27** has precedence.<sup>20</sup> The indicated sequential circumambulatory bond migration processes within **27** and, then, **28** account for loss of carbon

monoxide and lactone formation to produce compound **19** from each of the diastereomers **6–8**.

## Conclusions

An unusual decarbonylation reaction (of penam acids **5** and **7** to produce **9** and *epi-9*) has been studied. The proposed mechanism (Scheme 1) to account for the formation of thiazoline **9** is supported by detection of ca. 1 equiv of carbon monoxide (HRMS headspace analysis) that is produced upon heating the methyl ester **1** (the precursor of acid **5**) with LiI in EtOAc. Carbon monoxide formation was also observed when acid **7** was refluxed alone in EtOAc. Computations using the density functional theory method IEFPCM/M06/6-31+G(d) show that the activation free energies for the rate-limiting step in the decarbonylation of (the protonated form of) **7'** and **5'** are 17.2 and 8.8 kcal/mol, respectively, consistent with the fact that **7** was isolable and **5** was not. Thermal gas-phase reaction products produced during gas chromatographic analysis of the penam esters **1–4** and acids **6–8** (i.e., products **13–19** in Table 2) were deduced using high-resolution EI and CI mass spectrometry. Mechanistic pathways to account for these products are proposed (Schemes 2–4).

## Experimental Section

For full spectroscopic characterization data of compounds **1–4**, **6–8**, and **9** see ref 1. The preparation of **6**, **2**, and **4** (following closely the methods described in ref 3) and the demethylation of **4** to **8** (cf. reference 4) with LiI are provided here as representative procedures.

**(2S,5R,6R)-6-(1,3-Dihydro-1,3-dioxo-2H-isoindol-2-yl)-3,3-dimethyl-7-oxo-4-thia-1-azabicyclo[3.2.0]heptane-2-carboxylic Acid (6)**. 6-Aminopenicillanic acid (6-APA, 9.38 g, 41.6 mmol) was stirred vigorously in water (63 mL) at room temperature under an atmosphere of nitrogen. Sodium carbonate (6.00 g, 49.9 mmol) was added portionwise, producing a straw-colored solution. Finely ground *N*-carboethoxyphthalimide (9.49 g, 41.6 mmol) was added in a single portion and the mixture was stirred for 2.5 h. The reaction solution was then extracted with CH<sub>2</sub>Cl<sub>2</sub> (2 × 60 mL). Methylene chloride (60 mL) was added to the aqueous layer, and this mixture was swirled while being acidified by the addition of 1 M HCl (100 mL). After degassing was complete, the organic layer was removed and the aqueous phase extracted twice more with CH<sub>2</sub>Cl<sub>2</sub> (2 × 60 mL). The combined organic phases were washed with water (1 × 30 mL) and saturated brine (1 × 30 mL), dried with MgSO<sub>4</sub>, and filtered. Crystallization occurred during in vacuo evaporation of the solvent. The crystallized material was slurried in a minimal amount of diethyl ether and filtered to give **6** (4.82 g, 34%) as a white solid.

**(2S,5R,6R)-6-(1,3-Dihydro-1,3-dioxo-2H-isoindol-2-yl)-3,3-dimethyl-7-oxo-4-thia-1-azabicyclo[3.2.0]heptane-2-carboxylic Acid, Methyl Ester (2)**. Acid **6** (30 g, 86.6 mmol) was stirred in DMF (150 mL) at room temperature under an atmosphere of nitrogen. Triethylamine (12.1 mL, 86.6 mmol) was added dropwise followed by a dropwise addition of methyl iodide (5.9 mL, 95.3 mmol). The resulting yellow solution was allowed to stir for 5 h at room temperature. The progress of the reaction was monitored with TLC (silica gel, EtOAc/hexane, 1:1). The reaction solution was added to vigorously stirred ice water (750 mL) and extracted with CHCl<sub>3</sub> (750 mL). The organic layer was washed with saturated NaHCO<sub>3</sub> (3 × 750 mL) and saturated brine (750 mL), dried with MgSO<sub>4</sub>, and filtered. Crystallization occurred during in vacuo evaporation of the solvent. The crystallized material was slurried

in a minimal amount of diethyl ether and filtered to give **2** (13.0 g, 42%) as a white solid.

**(2S,5R,6S)-6-(1,3-Dihydro-1,3-dioxo-2H-isoindol-2-yl)-3,3-dimethyl-7-oxo-4-thia-1-azabicyclo[3.2.0]heptane-2-carboxylic Acid, Methyl Ester (4)**. Ester **2** (10.0 g, 27.8 mmol) was stirred in CH<sub>2</sub>Cl<sub>2</sub> (100 mL) at room temperature under an atmosphere of nitrogen. 1,8-Diazabicyclo[5.4.0]undec-7-ene (DBU, 0.3 mL, 1.9 mmol) was added dropwise and the solution was stirred for 90 min at ambient temperature. Saturated NH<sub>4</sub>Cl solution (100 mL) was added. The organic phase was washed with a saturated NH<sub>4</sub>Cl solution (2 × 100 mL), water (100 mL), and saturated brine (100 mL), dried with MgSO<sub>4</sub>, filtered, and concentrated in vacuo to give **4** (9.2 g, 92%) as a pale-yellow solid. The starting epimer **2** was not detectable in the <sup>1</sup>H NMR spectrum of this sample.

**(2S,5R,6S)-6-(1,3-Dihydro-1,3-dioxo-2H-isoindol-2-yl)-3,3-dimethyl-7-oxo-4-thia-1-azabicyclo[3.2.0]heptane-2-carboxylic acid (8)**. Ester **4** (5.0 g, 13.9 mmol) was stirred in EtOAc (150 mL) under an atmosphere of nitrogen. Anhydrous LiI (6.1 g, 45.5 mmol) was added and the mixture was stirred under reflux for 21 h. The solution was cooled and extracted with 5% NaHCO<sub>3</sub> (150 mL). Methylene chloride (150 mL) was added to the aqueous layer, which was slowly acidified by addition of 1 N HCl (150 mL). The aqueous layer was extracted with an additional portion of CH<sub>2</sub>Cl<sub>2</sub> (150 mL). The extracts were combined, washed with saturated brine (75 mL), separated, dried with MgSO<sub>4</sub>, and filtered. Concentration in vacuo gave **8** (2.1 g, 44%) as a white solid.

**Preparation of [S-(R\*,R\*)]-α-(2,5-Dihydro-5,5-dimethyl-2-thiazolyl)-1,3-dihydro-1,3-dioxo-2H-isoindole-2-acetic Acid (9)**. Ester **1** (0.10 g, 0.28 mmol) was stirred in EtOAc (3 mL) under an atmosphere of nitrogen in the apparatus shown in Figure 2. Anhydrous LiI (0.15 g, 1.1 mmol) was added and the mixture was stirred/refluxed for 22 h. The reaction solution was cooled and then extracted with 5% NaHCO<sub>3</sub> (3 mL). Methylene chloride (6 mL) was added to the aqueous layer and acidified by addition of 1 N HCl (3 mL) while stirring. The aqueous layer was extracted again with CH<sub>2</sub>Cl<sub>2</sub> (6 mL). The combined extracts were washed with water (6 mL), washed with saturated brine (6 mL), dried with MgSO<sub>4</sub>, and filtered. Evaporation in vacuo gave **9** (0.06 g, 72%) as a pale yellow solid. <sup>1</sup>H NMR (2 wt %/vol, CDCl<sub>3</sub>, 500 MHz) δ 1.54 (s, 3H, Me), 1.57 (s, 3H, Me), 4.83 (d, 1H, *J* = 9.9 Hz, H2), 6.26 (dd, 1H, *J* = 9.6, 2.3 Hz, H2'), 7.21 (d, 1H, *J* = 2.1 Hz, H4'), 7.71 (m, 2H, Ar<sub>meta</sub>), 7.83 (m, 2H, Ar<sub>ortho</sub>); <sup>13</sup>C NMR δ 29.0 (Me), 30.0 (Me), 57.9 (C2), 64.4 (C5'), 79.0 (C2'), 123.9 (Ar<sub>ortho</sub>), 131.8 (Ar<sub>ipso</sub>), 134.4 (Ar<sub>meta</sub>), 167.1 (Ar C=O), 170.8 (CO<sub>2</sub>H), 173.4 (C4'); HRMS calcd for C<sub>15</sub>H<sub>14</sub>N<sub>2</sub>O<sub>4</sub>SNa (M + Na) 341.0566, found 341.0560.

**Mass Spectrometric Analysis of Decarbonylation Reaction Headspace**. Headspace carbon monoxide was measured in the positive detection mode with a single cylindrical cell Fourier transform mass spectrometer equipped with a 3 T superconducting magnet. The background pressure of the cell was less than 10<sup>-10</sup> Torr. Ionization of the sample gases was performed by using a standard EI technique with a voltage of 60 eV.

In headspace analysis experiments a solution of ester **1** (ca. 0.1 g) in ethyl acetate (3 mL) and an excess (ca. 4-fold) of anhydrous LiI were combined in the apparatus diagrammed in Figure 2. The system was closed to prevent headspace exchange and then heated (90 °C, external bath) for ca. 24 h. The cooled apparatus was connected to the mass spectrometer inlet via T2, and valve two (V2) was opened to admit the headspace contents to the pre-evacuated ballast. The ballast contents were then leaked into the MS. The only neutral gaseous component identified was carbon monoxide and, specifically, carbon dioxide was not detected. In the experiment used to quantify the amount of CO produced, the solution of **1** (0.10 g, 0.28 mmol) was pretreated with a known amount of <sup>13</sup>CO (4.48 mL, 1 atm, 0.183 mmol, introduced via gastight syringe). The subsequent analysis of peak intensities at 27.9944 (for <sup>12</sup>CO) vs 28.9987 (for <sup>13</sup>CO) amu provided the ratio

(20) Carlsen, L.; Egsgaard, H.; Jørgensen, F. S.; Nicolaisen, F. M. J. *Chem. Soc., Perkin Trans. II* **1984**, 609–613.

of 1.6, which translates to 99% of the theoretical amount of carbon monoxide.

**Mass Spectrometric Analysis of Products from Thermal Decomposition during Gas Chromatographic Analysis.** The gas chromatography low and high-resolution mass spectrometry (GC-MS) analyses were performed with use of a magnetic sector instrument, using both positive ion EI and CI ionization. The source temperature was set to 250 °C for EI and 150 °C CI. The acceleration voltage was 5000 V. A mass range of 35–650 amu was used for the low-resolution analysis and a 60 amu mass window was scanned for high-resolution analysis. Measurement resolution was 1000 (10% valley) for LR and 5000 (10% valley) for HR. The ionization voltage was 70 eV for EI and a 4% mixture of NH<sub>3</sub> in CH<sub>4</sub> was used for CI ionization. The GC column was a 30 m DB-5MS capillary column. The carrier gas was helium and the column flow rate was ~1.0 mL/min. The GC injection port and transfer line temperatures were each set at 250 °C. The GC temperature was held at 50 °C for 1.5 min and then ramped at 20 °C per min to 320 °C.

**Acknowledgment.** The authors thank Dr. Dana Reed and Mr. Sean Murray of the University Minnesota Department of Chemistry Mass Spectrometry facility for helpful discussion and services and Professor Steven Kass for access to FT-MS instrumentation. This work was supported in part by the National Science Foundation (C.J.C., CHE-0610183) and the National Cancer Institute, National Institutes of Health (T.R.H., CA-76497).

**Supporting Information Available:** The <sup>1</sup>H and <sup>13</sup>C NMR spectra and a discussion of NMR peak assignments for **9** and the optimized conformer geometries, electronic energies, number of imaginary frequencies (if applicable) for **5'a** through **5'f** and **7'a** through **7'f** are provided. This material is available free of charge via the Internet at <http://pubs.acs.org>.

JO7023834